Neural firing rate model with a steep firing rate function

Muhammad Yousaf[a,c], Arcady Ponosov[a,b], John Wyller[a,*], Gaute T. Einevoll[a]

[a] *Department of Mathematical Sciences and Technology, Norwegian University of Life Sciences, P.O. Box 5003, N-1432 Ås, Norway*
[b] *Department of Mathematical Sciences, Florida Institute of Technology, Melbourne, FL 32901, USA(current address).*
[c] *Department of Mathematics, COMSATS Institute of Information Technology, Lahore, Pakistan.*

Abstract

In this study we justify rigorously the approximation of the steep firing rate functions with a unit step function in a two-population neural firing rate model with steep firing rate functions. We do this justification by exploiting the theory of switching dynamical systems. It has been demonstrated that switching dynamics offer a possibility of simplifying the dynamical system and getting approximations of the solution of the system for any specific choice of parameters. In this approach the phase space of the system is divided into regular and singular domains, where the limit dynamics can be written down explicitly. The advantages of this method are illustrated by number of numerical examples for different cases of the singular domains (i.e. for black, white and transparent walls) and for specific choices of parameters involved. General conditions have been formulated on these parameters to give black, white and transparent walls. Further, the existence and stability of regular and singular stationary points have been investigated. It has been shown that the regular stationary points (i.e. stationary points inside the regular domains) are always stable and this property is preserved for smooth and sufficiently steep activation functions. In the most technical part of the paper we have provided conditions on the existence and stability of singular stationary points (i.e. those belonging to the singular domains). For the

*Corresponding Author: Tel. +47 64965489; fax.+47 64965401.
Email address: john.wyller@umb.no (John Wyller)

existence results, the implicit function theorem has been used, whereas the stability of singular stationary points is addressed by applying the singular perturbation analysis and the Tikhonov theorem.

Keywords: Two population firing rate model, Switching dynamics, Regular and singular domains, Singular perturbation analysis, Implicit function theorem and Tikhonov theorem.

---

1. Introduction

Neurons carry information from one part of the brain to another, which can be described by various types of mathematical models [1, 2, 3, 4, 5, 6, 7]. The firing rate models have the coarsest level of detail. Here the probability for firing action-potential is modeled. Existing firing rate models consist of sets of differential equations, e.g. for synaptic-drive models [8, 9, 10, 11, 12] each of the differential equations has the following general form:

$$\tau_j \frac{du_j}{dt} = -u_j + P_j \left(\sum_k \omega_{jk} u_k \right) \tag{1}$$

Here u_j is the synaptic drive from the neuron j, ω_{jk} is the synaptic weight from the presynaptic element k to the post synaptic element j, τ_j is the time constant representing the decay of the synaptic drive u_j following the action potential in the element j. The function P_j represents the firing-rate function converting the net synaptic drive to the firing rate [8, 10]. These firing rate functions are given as sigmoidal functions i.e. they constitute a one - parameter family of increasing functions in the state variables, parameterized by the steepness of the function, they assume values between 0 and 1 and they approach the unit step function in the limit of infinite steepness.

Rate equation models also occur in other branches of mathematical biology, for example in the study of gene regulatory networks [13, 14, 15, 16, 17, 18, 19]. A simple gene regulatory network model is given as

$$\frac{dy_i}{dt} = F_i(Z_1, Z_2, ..., Z_n) - G_i(Z_1, Z_2, ..., Z_n) y_i, \quad i = 1, 2, ..., n, \tag{2}$$

and the functions F_i and G_i are the production and the relative degradation rates of gene i, respectively, and y_i stands for the gene product concentrations. The functions Z_j which are referred to as the activation functions are

modeled by means of sigmoidal functions, just as as the firing rate functions in the model (1). The model (2) has been studied in this limit in [13, 14, 20]. In this case the right hand side of (2) possesses jump discontinuities along certain surfaces in the phase space. These surfaces are referred to as the singular domains of the dynamical system. In the rest of the phase space (referred to as the regular domains), the dynamical system (2) turns into a system of coupled linear differential equations.

The problem studied in those papers consists in proving uniform convergence of the solutions of (2) when the threshold functions become infinitely steep. This gives, in particular, an algorithm of gluing the limit solutions in the regular domains together with those in the singular domains. The key tool in this analysis is the theory of switching dynamical systems and singular perturbation theory [13, 14].

This serves as a background for the present study. Our aim is to justify rigorously the approximation of the steep firing rate functions with a unit step function in the firing rate model (1). We do this justification in a way analogous to [13, 14]] for the gene regulatory networks of the type (2).

The paper is organized in the following way:

In section 2, we introduce the two-population (excitatory and inhibitory) firing-rate model and derive an autonomous dynamical system using linear chain trick [8, 21, 22]. In section 3, we establish the platform to investigate the dynamics of the two population firing rate model using the theory of switching dynamical systems. Some notions from this theory are defined in this section, e.g. regular domains, singular domains and stationary points corresponding to these domains (regular and singular stationary points). We transform the actual dynamical system from the (u_e, u_i)–coordinates to the new net input variables (x, y) in section 4. This transformation makes it possible to perform the stability analysis of the singular stationary point using singular perturbation theory. Next, in section 5, the existence of regular stationary points (RSP) and singular stationary points (SSP) are addressed. We explore the existence of regular stationary points for finitely steep activation functions. We also formulate the conditions on the parameters providing the existence of singular stationary points. In section 6, we investigate the asymptotic stability of regular and singular stationary points. We also study

the dynamics along black walls by applying singular perturbation theory and the Tikhonov theorem [23, 24]. Section 7 contains main conclusions and an outlook.

2. Model

The starting point is the simplified two-population synaptic drive model with excitatory and inhibitory activities given by the Volterra equations

$$u_e = \alpha_e * Z_e(\omega_{ee}u_e - \omega_{ei}u_i) \tag{3a}$$

$$u_i = \alpha_i * Z_i(\omega_{ie}u_e - \omega_{ii}u_i), \tag{3b}$$

where

$$(\alpha_m * Z_m(x))(t) = \int_{-\infty}^{t} \alpha_m(t-s)Z_m(x(s))ds. \tag{4}$$

Here α_m for $m = e, i$ are the temporal kernels showing the impact of past neural firing on the present activity levels in the network [8, 11, 12]. These kernels are typically parameterized by a single time constant. In this study the temporal kernels are modeled by means of exponentially decaying functions

$$\alpha_e(t) = \exp(-t) \ \ , \ \ \alpha_i(t) = \frac{1}{\tau}\exp(-\frac{t}{\tau}). \tag{5}$$

The functions u_m for $m = e, i$ in (3) are the average activity levels for excitatory and inhibitory populations. τ is the relative inhibition time which is given as the ratio between inhibitory to excitatory time constants. The connectivity parameters ω_{mn} $(m = e, i)$ model the connection strength (from n to m cells) in the network. In this study, the parameters are assumed to satisfy the following conditions:

$$0 < \omega_{mn} \leq 1, \ \ 0 < \theta_m \leq 1, \ \tau > 0. \tag{6}$$

The activation function Z_m for $m = e, i$ is modeled by

$$Z_m(x_m) = H(q_m, \theta_m, x_m) = \begin{cases} 0 & x_m < 0 \\ \frac{x_m^{1/q_m}}{x_m^{1/q_m} + \theta_m^{1/q_m}} & x_m \geq 0, \end{cases} \tag{7}$$

where H is called the Hill function. The parameter θ_m gives the threshold

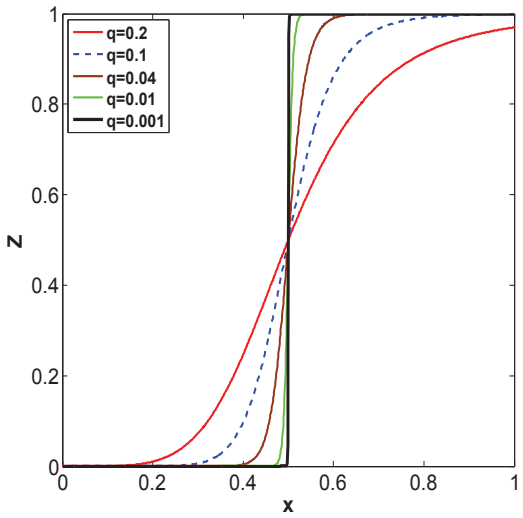

Figure 1: The Hill function for different values of the steepness parameter q at $\theta = 0.5$.

values, while q_m for $m = e, i$ measures the steepness of the firing rate function and it is assumed to satisfy $0 < q_m \leq 1$. In Fig.1 the Hill function is plotted for different values of the steepness parameter q for a fixed threshold value $\theta = 0.5$ (for a detailed review see [18, 25]). For the sake of simplicity, we assume that $q_e = q_i = q$. The system of Volterra equations (3) can be converted to a 2D autonomous dynamical system by means of the linear chain trick [8, 21, 22] using exponentially decaying temporal kernels (5):

$$u_e' = -u_e + Z_e(\omega_{ee}u_e - \omega_{ei}u_i) \tag{8a}$$

$$\tau u_i' = -u_i + Z_i(\omega_{ie}u_e - \omega_{ii}u_i). \tag{8b}$$

For convenience, we write the model (8) in the vector form as

$$\underline{\mathbf{U}}' = \underline{\mathbf{F}}(\underline{\mathbf{U}}), \quad \underline{\mathbf{F}}(\underline{\mathbf{U}}) = -\mathbf{D}\ \underline{\mathbf{U}} + \mathbf{D}\ \underline{\mathbf{G}}(\mathbf{\Omega}\underline{\mathbf{U}}), \tag{9}$$

where

$$\mathbf{D} = \begin{bmatrix} 1 & 0 \\ 0 & \tau^{-1} \end{bmatrix}, \ \underline{\mathbf{U}} = \begin{bmatrix} u_e \\ u_i \end{bmatrix}, \ \mathbf{\Omega} = \begin{bmatrix} \omega_{ee} & -\omega_{ei} \\ \omega_{ie} & -\omega_{ii} \end{bmatrix} \tag{10}$$

and

$$\underline{\mathbf{G}}(\mathbf{\Omega}\underline{\mathbf{U}}) = \begin{bmatrix} Z_e(\omega_{ee}u_e - \omega_{ei}u_i) \\ Z_i(\omega_{ie}u_e - \omega_{ii}u_i). \end{bmatrix} \tag{11}$$

The model (8), or equivalently the system (9)-(11), constitutes the basis of the present study.

2.1. Wellposedness

The vector function $\underline{\mathbf{F}}$ is continuously differentiable with respect to the steepness parameter $q > 0$. Hence the initial value problem for (8) is locally wellposed. In order to prove global wellposedness of the initial value problem for (8), it will be sufficient to show that the vector function $\underline{\mathbf{F}}$ is bounded by some linear function. The nonlinear part of the vector function $\underline{\mathbf{F}}$ is the Hill function which is always bounded for the finite positive steepness $\mathtt{q}$. Since both eigenvalues of the matrix $\mathbf{D}$ are negative ($\lambda_1 = -1 < 0$, $\lambda_2 = -\frac{1}{\tau} < 0$) and the nonlinear part of $\underline{\mathbf{F}}$ is bounded for a finite positive q, we get

$$|\mathbf{D}\underline{\mathbf{G}}(\Omega\underline{\mathbf{U}})| \leq ||\mathbf{D}|| \cdot |\underline{\mathbf{G}}(\mathbf{\Omega}\underline{\mathbf{U}})| \leq \ c_1, \tag{12}$$

where $||.||$ is the matrix norm and c_1 is some positive constant. Similarly, the linear part of the function $\underline{\mathbf{F}}$ is also bounded

$$|\mathbf{D}\ \underline{\mathbf{U}}| \ \leq ||\mathbf{D}|| \cdot |\underline{\mathbf{U}}| \leq \ \ c_2 \cdot |\underline{\mathbf{U}}|, \tag{13}$$

where c_2 is also some positive constant. Combining (12) and (13) yields

$$|\underline{\mathbf{F}}(\underline{\mathbf{U}})| \leq c_1 + c_2 \cdot |\underline{\mathbf{U}}|, \tag{14}$$

which shows that the vector function $\underline{\mathbf{F}}$ is bounded by some linear function $c_1 + c_2 \cdot \underline{\mathbf{U}}$. Hence, the initial value problem (8) is globally wellposed.

3. Regular and singular domains

In this section, we first introduce the notions of regular and singular domains with corresponding focal points in the phase space of the dynamical system (8). Then, we give examples of three different versions of the singular domains (black, white and transparent walls) by varying the parameters ω_{mn} and θ_m.

In the limit $q \to 0$, the Hill function (7) becomes the Heaviside step function S:

$$S(x_m) = \begin{cases} 1, & x_m > \theta_m \\ \frac{1}{2}, & x_m = \theta_m \\ 0, & x_m < \theta_m \end{cases} \qquad (\mathrm{m} = e, i). \tag{15}$$

The threshold lines for the dynamical system (8) are defined as the discontinuity lines

$$L_e : \omega_{ee} u_e - \omega_{ei} u_i = \theta_e \tag{16a}$$

$$L_i : \omega_{ie} u_e - \omega_{ii} u_i = \theta_i. \tag{16b}$$

The dynamical system (8) with the step function (15) has the following features:

The vector function $\underline{\mathbf{F}}$ is discontinuous on the threshold lines L_m for $m = e, i$, which are also called switching domains, singular domains, or walls [14, 20, 25]. These walls divide the phase space of (8) into four different regions called regular domains. In each of the four regular domains the vector function $\underline{\mathbf{F}}$ becomes linear (with constant coefficients). In each regular domain, all the trajectories of the system move toward a point attractor called the focal point of the corresponding regular domain (see [14, 20, 25] for further details).

The representation (15) naturally divides the (u_e, u_i) plane into four disjoint regular domains denoted by Ω_1, Ω_2, Ω_3 and Ω_4:

$$\Omega_1 = \{(u_e, u_i) \mid \omega_{ee} u_e - \omega_{ei} u_i < \theta_e \ , \ \omega_{ie} u_e - \omega_{ii} u_i < \theta_i\}, \tag{17a}$$

$$\Omega_2 = \{(u_e, u_i) \mid \omega_{ee} u_e - \omega_{ei} u_i > \theta_e \ , \ \omega_{ie} u_e - \omega_{ii} u_i < \theta_i\}, \tag{17b}$$

$$\Omega_3 = \{(u_e, u_i) \mid \omega_{ee} u_e - \omega_{ei} u_i < \theta_e \ , \ \omega_{ie} u_e - \omega_{ii} u_i > \theta_i\}, \tag{17c}$$

$$\Omega_4 = \{(u_e, u_i) \mid \omega_{ee} u_e - \omega_{ei} u_i > \theta_e \ , \ \omega_{ie} u_e - \omega_{ii} u_i > \theta_i\}. \tag{17d}$$

The regular and singular domains in (u_e, u_i) plane corresponding to (17) are displayed in Fig.2.

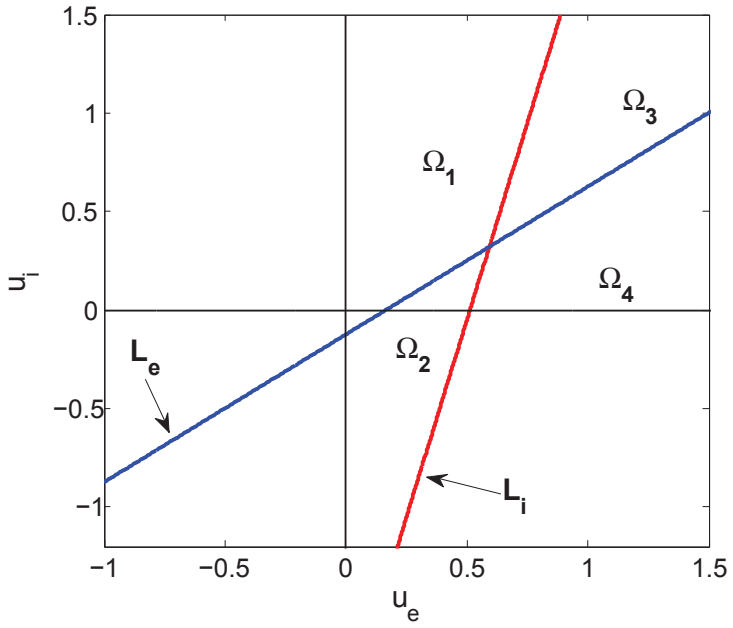

Figure 2: Regular and singular domains of the system (8). The regular domains Ω_1, Ω_2, Ω_3 and Ω_4 are given by (17). The singular domains L_e and L_i given by (16) are marked as blue and red lines, respectively. Input data for the plot: $\omega_{ee} = 0.6$, $\omega_{ei} = 0.8$, $\omega_{ie} = 0.8$, $\omega_{ii} = 0.2$, $\theta_e = 0.1$ and $\theta_i = 0.4$.

By combining (8) and (15), we get four dynamical systems corresponding to the four regular domains (17):

$$u_e' = -u_e \ , \ \tau u_i' = -u_i, \ \ (u_e, u_i) \in \Omega_1, \tag{18a}$$

$$u_e' = -u_e + 1 \ , \ \tau u_i' = -u_i, \ \ (u_e, u_i) \in \Omega_2, \tag{18b}$$

$$u_e' = -u_e \ , \ \tau u_i' = -u_i + 1, \ \ (u_e, u_i) \in \Omega_3, \tag{18c}$$

$$u_e' = -u_e + 1 \ , \ \tau u_i' = -u_i + 1, \ \ (u_e, u_i) \in \Omega_4. \tag{18d}$$

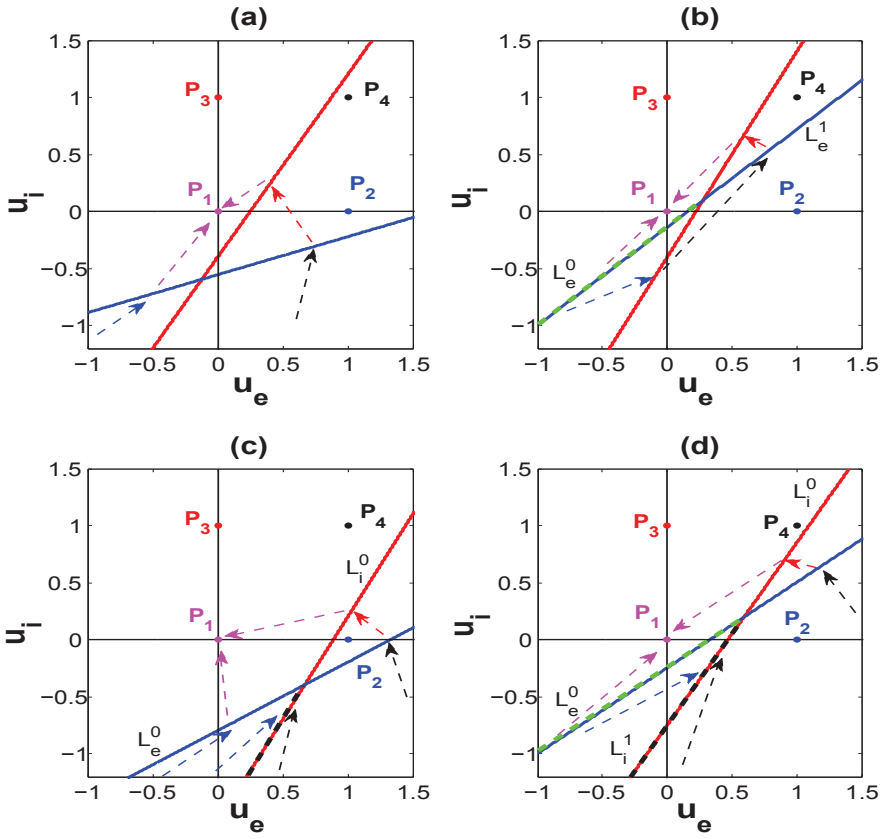

Figure 3: Interpretation of the singular domains L_i (red) and L_e (blue) as white, transparent and black for the parameter sets given in Table 1. White and black walls are marked with green and black colors (dashed), respectively. The integral curves in each regular domain are represented by dashed arrows. (a) Transparent walls for the parameter set A. (b) Transparent and white walls for the parameter set B. (c) Transparent and black walls for the parameters set C (d) Transparent, white and black walls for the parameters set D in the Table 1.

The focal points corresponding to the dynamical systems (18) are given as

$$P_1 = (0,0) \quad P_2 = (1,0) \ , \ P_3 = (0,1) \ , \ P_4 = (1,1), \tag{19}$$

respectively. The location of the focal points P_1, P_2, P_3 and P_4 relative to the

threshold lines L_e and L_i determines the behavior of solutions (see [14, 17, 18, 20, 26] for further details).

Definition 1. *A subset of the singular domain L_m $(m = e, i)$ is said to be a* black wall*, if all the trajectories from both sides of the wall are attracted toward the wall.*

Definition 2. *A subset of the singular domain L_m $(m = e, i)$ is said to be a* white wall *if all the trajectories are repelled from both sides of the wall.*

Definition 3. *A subset of the singular domain L_m $(m = e, i)$ is said to be* transparent wall*, if the trajectories cross the wall.*

For the sake of simplicity, we further divide each of the singular domains L_e and L_i into two parts.

Definition 4. *The line segment L_e^0 consists of points satisfying*

$$L_e^0 = \{(u_e, u_i) \mid \omega_{ee}u_e - \omega_{ei}u_i = \theta_e\ ,\ \ \omega_{ie}u_e - \omega_{ii}u_i < \theta_i\}, \tag{20a}$$

while the line segment L_e^1 satisfy the conditions

$$L_e^1 = \{(u_e, u_i) \mid \omega_{ee}u_e - \omega_{ei}u_i = \theta_e\ ,\ \ \omega_{ie}u_e - \omega_{ii}u_i > \theta_i\}. \tag{20b}$$

Definition 5. *The line segment L_i^0 consists of points satisfying*

$$L_i^0 = \{(u_e, u_i) \mid \omega_{ee}u_e - \omega_{ei}u_i < \theta_e\ ,\ \ \omega_{ie}u_e - \omega_{ii}u_i = \theta_i\}, \tag{21a}$$

while line segment L_i^1 satisfy the conditions

$$L_i^1 = \{(u_e, u_i) \mid \omega_{ee}u_e - \omega_{ei}u_i > \theta_e\ ,\ \ \omega_{ie}u_e - \omega_{ii}u_i = \theta_i\}. \tag{21b}$$

Fig. 3 shows examples of black, white and transparent walls. In Fig. 3d the red line segment dashed with black color (L_i^1) is a black wall. The remaining part of this red line is denoted by L_i^0 and is a transparent wall. The blue line dashed with green color (L_e^1) is a white wall, whereas the remaining part of this line (L_e^0) is a transparent wall.

Next, we formulate conditions for a wall to be black, white and transparent.

Proposition 1. ***(Conditions for black walls)***

1. *The singular domains L_i^0 and L_e can never be black walls.*
2. *L_i^1 is black if*

$$\omega_{ie} - \omega_{ii} < \theta_i < \omega_{ie}. \tag{22}$$

Proposition 2. ***(Conditions for white walls)***

1. *L_e^0 is a white wall if*

$$\omega_{ee} > \theta_e. \tag{23}$$

2. *L_e^1 is white wall if*

$$\omega_{ee} - \omega_{ei} > \theta_e. \tag{24}$$

3. *The wall L_i can never be white.*

Proposition 3. ***(Conditions for transparent walls)***

1. *The singular domain L_i^0 is always a transparent wall.*
2. *L_i^1 is a transparent wall if*

$$\omega_{ie} < \theta_i \tag{25a}$$

or

$$\omega_{ie} - \omega_{ii} > \theta_i. \tag{25b}$$

3. *L_e^0 is a transparent wall if*

$$\omega_{ee} < \theta_e. \tag{26}$$

4. *L_e^1 is a transparent wall if*

$$\omega_{ee} - \omega_{ei} < \theta_e. \tag{27}$$

The proofs of Proposition 1, Proposition 2 and Proposition 3 proceed in the same way. We prove Proposition 1 and omit the proofs of Proposition 2 and Proposition 3.

Proof.

1. *In this case the regular domain Ω_1 containing the focal point $P_1(0,0)$ is bounded by the walls L_i^0 and L_e^0. All integral curves in the regular domain Ω_1 move away from these walls and are attracted toward the focal point P_1. Hence, the walls L_i^0 and L_e^0 can never be black. The only possibility for L_e^1 to be black is that*

$$\omega_{ee} - \omega_{ei} < \theta_e < -\omega_{ei}. \tag{28}$$

However, the condition (28) is not fulfilled for the present choice of the parameters (6). Hence, the wall L_e^1 can never be black.

2. *The wall L_i^1 is black if the focal point corresponding to the right side regular domain Ω_2 of the wall is to be found in the left side regular domain (Ω_4) of the wall and vice versa. This results in the phase portrait where all integral curves in these regular domains move toward the wall L_i^1. In order to produce this scenario, the parameters ω_{ie}, ω_{ii} and θ_i must satisfy the inequality (22).*

Parameters	ω_{ee}	ω_{ei}	ω_{ie}	ω_{ii}	θ_e	θ_i
Set A	0.3	0.9	0.8	0.5	0.5	0.2
Set B	0.6	0.6	0.9	0.5	0.1	0.2
Set C	0.3	0.5	0.9	0.5	0.4	0.8
Set D	0.3	0.4	0.32	0.2	0.1	0.15

Table 1: Sets of parameters used to demonstrate different behaviors of singular domains. The parameter set A is used to demonstrate the transparent wall behavior. The set B produces transparent and white walls. The set C is used to produce transparent and black walls, while the set D generates black, white and transparent walls at the same time.

We summarize the results obtained in Proposition 1, Proposition 2 and Proposition 3 in the phase plots of Fig. 4. From this figure we can infer that the singular domain L_e^0 can never be a black wall. It becomes a white wall for $\omega_{ee} > \theta_e$ and a transparent wall for $\omega_{ee} < \theta_e$. The wall L_e^1 behaves in the similar fashion as L_e^0: it is a transparent wall for $\omega_{ee} - \omega_{ei} < \theta_e$ and a white wall for $\omega_{ee} - \omega_{ei} > \theta_e$. The singular domain L_i^0 is always a transparent

wall, while the wall L_i^1 is black for the parameter regime $\omega_{ie} - \omega_{ii} < \theta_i < \omega_{ie}$ and transparent otherwise.

The parameter sets $A - D$ in the table 1 give rise to different types of the singular domains in accordance with the Proposition 1 - Proposition 3. In Fig. 3, the singular domains L_i and L_e are represented by the red and blue color lines, respectively. The direction of integral curves in each of the regular domains is represented by different color directed arrows (dashed). The corresponding focal points (19) for each of the four regular domains are also indicated with four different color dots.

More specifically, we have following behavior types of the singular domains L_e and L_i for the parameter sets A-D in Table 1:

1. Both of the singular domains L_e and L_i are transparent walls for the parameter set A in Table 1 (Fig. 3a).

2. The line segment L_e^0 of L_e dashed with green color is a white wall, whereas the remaining line segments L_e^1 and L_i are transparent for the parameter set B in Table 1 (Fig. 3b).

3. The line segment L_i^1 of L_i dashed with black color stands for a black wall, whereas the rest of line segments L_e and L_i^0 are transparent walls for the parameter set C in Table 1 (see Fig. 3c).

4. The line segments L_e^0 and L_i^1 are a white and black wall, respectively, while the line segments L_i^0 and L_e^0 are transparent walls for the parameter set D in Table 1 (Fig. 3d).

We conclude this section with discussing the notion of a stationary point (steady state) for the system (8). An immediate adaptation of this notion to our case gives the following definition:

Definition 6. *A point $P_0(u_e^0, u_i^0)$ is said to be a stationary point of the dynamical system (8) if*

$$-u_e^0 + Z_e(\omega_{ee}u_e^0 - \omega_{ei}u_i^0) = 0 \tag{29a}$$

$$-u_i^0 + Z_i(\omega_{ie}u_e^0 - \omega_{ii}u_i^0) = 0. \tag{29b}$$

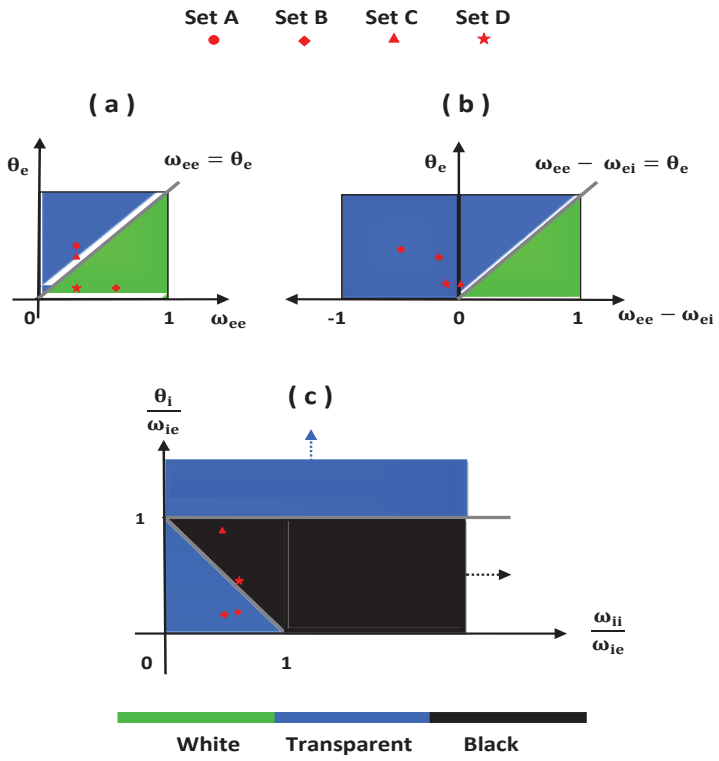

Figure 4: Phase plots based on the results obtained in Proposition 1, Proposition 2 and Proposition 3 showing the parameter regimes for the black, white and transparent walls. The parameter sets A-D are also marked in these phase plots: (a) Parameter regimes for the wall L_e^0 to be white or transparent. (b) Parameter regimes for the wall L_e^1 to be white or transparent. (c) Parameter regimes for the wall L_i^1 to be black or transparent. The condition (22) for the black wall is equivalent with $1 - \frac{\omega_{ii}}{\omega_{ie}} < \frac{\theta_i}{\omega_{ie}} < 1$. The separatrices between the regions producing black and transparent walls are $\frac{\theta_i}{\omega_{ie}} = 1 - \frac{\omega_{ii}}{\omega_{ie}}$ and $\frac{\theta_i}{\omega_{ie}} = 1$.

However, this definition is only applicable if the threshold functions have finite steepness (i.e. smooth). If they are infinitely steep, the solution of the system (29) belongs to its continuity set, i.e. to one of the regular domains of the system (8). This justifies the following definition:

Definition 7. *The stationary point lying in one of the regular domains are*

called regular stationary points (RSP)

Yet, this definition is not alone sufficient for our purposes. For instance, it does not work in the case of black walls, which attracts the trajectories and therefore may also contain stationary points of the system. The coordinates of such stationary points cannot be determined from the system (29), as they belong to the discontinuity set of the right-hand side of the system (8). In this case, the idea is to define such stationary points (called singular in the sequel) as the limits of (proper) stationary points of the system (8) with finitely steep threshold functions letting the steepness parameter q go to 0 (see [18, 20] for the details). Then we arrive at the following definition:

Definition 8. *The stationary points lying in one of the singular domains are called singular stationary points (SSP)*

Let us only stress that this definition contains implicitly the requirement that the approximating stationary points (for small positive q) converge to a limit point belonging to a singular domain of the system (8). In Fig. 3d, some of the trajectories move toward $P_1(0,0)$ which is a regular stationary point of the system (8), while some other trajectories approach the black wall L_i^1 which is a red line dashed with black color. As the trajectories do not leave this wall, it must contain an attracting point which is a singular stationary point of the system (8). Note, however, that we cannot immediately find the coordinates of this point, as we have no information about the behavior of the trajectories in the black wall. The problem of finding the coordinates of a singular stationary point and the trajectories of the system in the black wall will be treated in the forthcoming sections.

4. The model in net input variables

In order to investigate the relationship between the evolution in the regular and the singular domains, we convert the dynamical system (8) into a dynamical system in the variables x and y defined as

$$x = \omega_{ee}u_e - \omega_{ei}u_i \ \ , \ \ y = \omega_{ie}u_e - \omega_{ii}u_i, \tag{30}$$

where it is assumed that $\omega_{ei}\omega_{ie} - \omega_{ee}\omega_{ii} \neq 0$. We refer to x and y as the *net input variables*. More specifically, the mapping from the actual activity variables (u_e, u_i) to the net input variables (x, y) is shown in Fig. 5. In

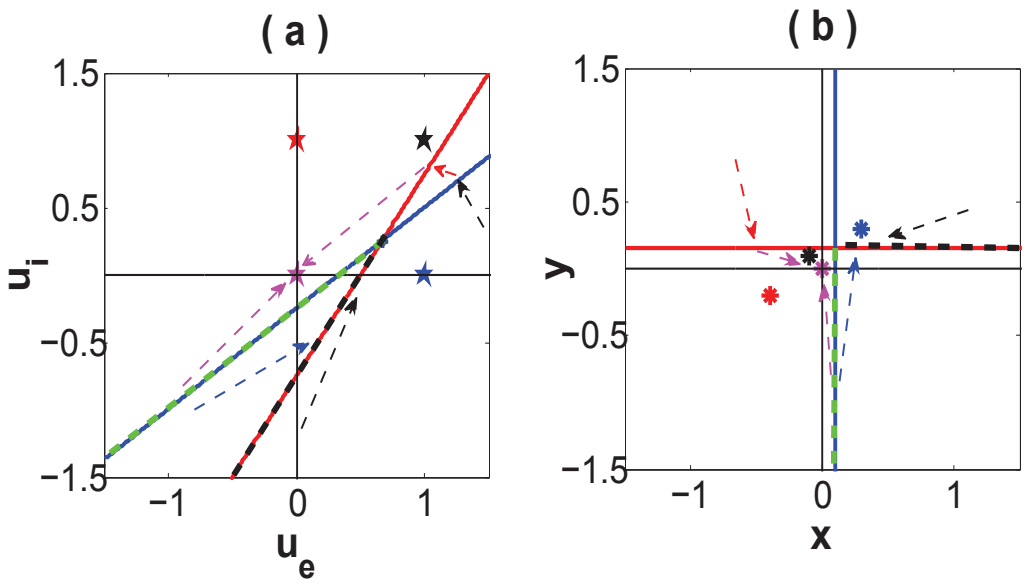

Figure 5: The mapping from the domain of the activity variables (u_e, u_i) to the domain of the net input variables (x, y) corresponding to Fig. 3d. The blue line segment dashed with green color and red line segment dashed with black color serve as white and black walls, respectively. The remaining line segments of singular domains constitute transparent walls. The integral curves in each regular domain are represented by dashed arrows. (a) Singular and regular domains with the corresponding focal points in the (u_e, u_i) plane. (b) Singular ($x = \theta_e$ and $y = \theta_i$) and regular domains with the corresponding focal points in the (x, y) marked with same color as in (a). The corresponding parameters are given by the set D in the Table 1.

Fig. 5b the red line ($y = \theta_i$) dashed with the black color represents a black wall, while the blue line ($x = \theta_e$) dashed with green color is a white wall. As we know, singular stationary points may exist in the case of black walls.

In the matrix form the system (8) is equivalent to

$$\underline{\mathbf{U}}' = -\mathbf{D}\,\underline{\mathbf{U}} + \mathbf{D}\,\underline{\mathbf{G}}(\underline{\mathbf{X}}), \tag{31}$$

where the matrices $\mathbf{D}$, $\underline{\mathbf{U}}$ are defined in (10) and $\underline{\mathbf{G}}$, $\underline{\mathbf{X}}$ are given as

$$\underline{\mathbf{X}} = \begin{bmatrix} x \\ y \end{bmatrix}, \; \underline{\boldsymbol{G}} = \begin{bmatrix} Z_e(x) \\ Z_i(y) \end{bmatrix}. \tag{32}$$

The transformation (30) can be expressed in the matrix form as

$$\underline{\mathbf{X}} = \mathbf{\Omega}\ \underline{\mathbf{U}}, \tag{33}$$

where $\mathbf{\Omega}$ is defined in (10). Now, using (33) and the fact that $\mathbf{\Omega}$ by assumption is invertible, we get

$$\mathbf{X}' = \mathbf{\Omega}\ (-\mathbf{D}\ \mathbf{\Omega}^{-1}\underline{\mathbf{X}} + \mathbf{D}\ \underline{\mathbf{G}}(\underline{\mathbf{X}})), \tag{34}$$

or

$$\underline{\mathbf{X}}' = \underline{\mathbf{Q}}\ (\underline{\mathbf{X}}), \quad \underline{\mathbf{Q}}\ (\underline{\mathbf{X}}) = \mathbf{A}\ \underline{\mathbf{X}} + \underline{\mathbf{B}}\ (\underline{\mathbf{X}}), \tag{35}$$

where

$$\mathbf{A} = -\mathbf{\Omega D}\ \mathbf{\Omega}^{-1}\ \ ,\ \ \underline{\mathbf{B}}\ (\underline{\mathbf{X}}) = \mathbf{\Omega}\ \mathbf{D}\ \underline{\mathbf{G}}\ (\underline{\mathbf{X}}). \tag{36}$$

The vector function $\underline{\mathbf{Q}}$ is given as

$$\underline{\mathbf{Q}}(q,x,y) = \begin{bmatrix} Q_1(q,x,y) \\ \\ Q_2(q,x,y) \end{bmatrix}, \tag{37}$$

where

$$Q_1(q,x,y) = \mu_1\ x\ + \nu_1\ y + \omega_{ee}\ Z_e(x) - \frac{1}{\tau}\ \omega_{ei}\ Z_i(y), \tag{38}$$

$$Q_2(q,x,y) = \mu_2\ x\ + \nu_2\ y + \omega_{ie}\ Z_e(x) - \frac{1}{\tau}\ \omega_{ii}\ Z_i(y), \tag{39}$$

so that the system (35) becomes

$$x' = Q_1(q,x,y) \tag{40a}$$

$$y' = Q_2(q,x,y). \tag{40b}$$

The coefficients μ_1, ν_1, μ_2 and ν_2 are defined as

$$\mu_1 \ = \ \frac{-\omega_{ei}\omega_{ie} + \tau\omega_{ee}\omega_{ii}}{\tau d},\ \ \nu_1 = \frac{\omega_{ee}\omega_{ei}(1-\tau)}{\tau d}, \tag{41a}$$

$$\mu_2 \ = \ \frac{\omega_{ie}\omega_{ii}(\tau-1)}{\tau d}, \quad \nu_2 = \frac{-\tau\omega_{ei}\omega_{ie} + \omega_{ee}\omega_{ii}}{\tau d}, \tag{41b}$$

$$d \ = \ \omega_{ei}\omega_{ie} - \omega_{ee}\omega_{ii}. \tag{41c}$$

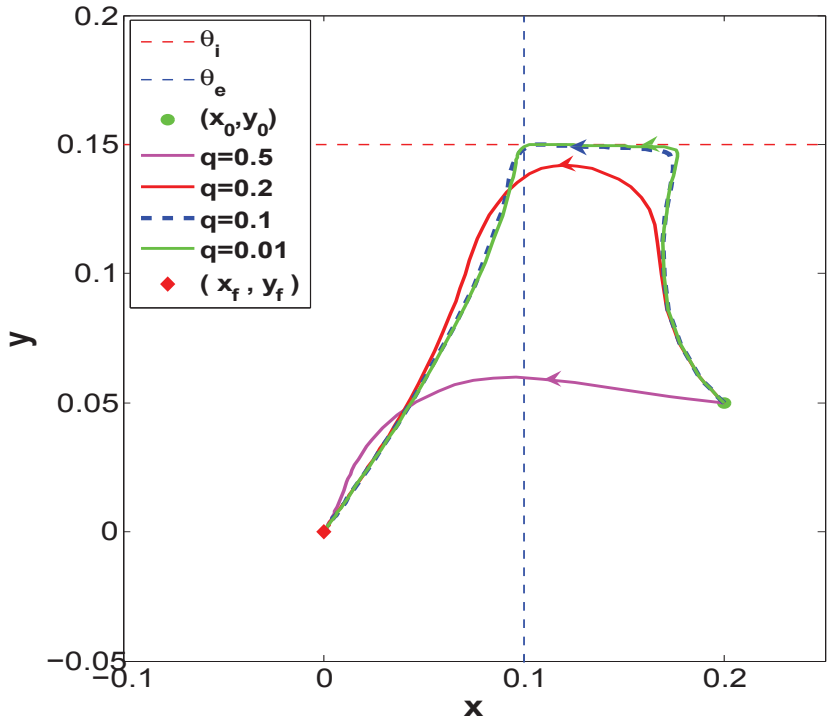

Figure 6: Integral curves of the dynamical system (40) for different steepness q and for the parameter set D in the Table 1, cf Fig. 1

The general formulae for the focal points of the system (40) are given as

$$
\begin{aligned}
P_1(x_1, y_1) &= (0, 0), && \text{(42a)}\\
P_2(x_2, y_2) &= ((\omega_{ie}\nu_1 - \omega_{ee}\nu_2)/c,\ (\omega_{ee}\mu_2 - \omega_{ie}\mu_1)/c), && \text{(42b)}\\
P_3(x_3, y_3) &= ((\omega_{ei}\nu_2 - \omega_{ii}\nu_1)/c\tau,\ (\omega_{ii}\mu_1 - \omega_{ei}\mu_2)/c\tau), && \text{(42c)}\\
P_4(x_4, y_4) &= ((x_2 + x_3,\ y_2 + y_3), && \text{(42d)}
\end{aligned}
$$

where $c = \mu_1\nu_2 - \mu_2\nu_1$. Fig. 6 shows the trajectories of the dynamical system (40) for different steepness parameters q. There is no black wall-like behavior if the steepness parameter q is sufficiently far from 0. As q approaches zero (i.e. when the steepness becomes infinitely large), the appearance of a black wall can be detected. The solutions approach this wall from both sides and a special technique is required to understand what happens to the solutions

in the wall.

5. Existence of regular and singular stationary points

In the previous section we showed how to rewrite the system (8) in the net input variables, which resulted in the equivalent system (40). In this section we use this representation to investigate the existence of stationary points for the system (40) (and thus for the system (8)) for small positive q and for $q = 0$ (the limit case). We start with the analysis of the stationary points that converge (as $q \to 0$) to a regular stationary point (RSP) in the sense of Definition 7.

Theorem 1. *Assume that for $q = 0$ the dynamical system (40) possesses a RSP $(x^\star, y^\star)$. Then there exists a positive $q_0 > 0$ such that for all $0 < q < q_0$ the system (40) has a stationary point $(x(q), y(q))$ which converges to the RSP $(x^\star, y^\star)$ as $q \to 0$.*

Proof. *We prove this theorem by using the implicit function theorem. We observe that the vector function $\underline{\boldsymbol{Q}}$ defined by (37) satisfies the following conditions:*

1. *$\underline{\boldsymbol{Q}} : \mathbb{R}_0^+ \times \mathbb{R}^2 \longrightarrow \mathbb{R}^2$ is a smooth vector function, where $\mathbb{R}_0^+ = [0, \infty)$.*

2. *By assumption, $\underline{\boldsymbol{Q}}(0, x^\star, y^\star) = \boldsymbol{O}$, where $(x^\star, y^\star)$ belongs to a regular domain.*

3. *The Jacobian $\boldsymbol{J}$ of the vector function $\underline{\boldsymbol{Q}}$ evaluated at $(0, x^\star, y^\star)$ is given as*

$$\boldsymbol{J} = \begin{bmatrix} \frac{\partial Q_1}{\partial x} & \frac{\partial Q_1}{\partial y} \\ \\ \frac{\partial Q_2}{\partial x} & \frac{\partial Q_2}{\partial y} \end{bmatrix} (0, x^\star, y^\star) = \begin{bmatrix} \mu_1 & \nu_1 \\ \\ \mu_2 & \nu_2 \end{bmatrix}, \tag{43}$$

   where μ_1, μ_2, ν_1 and ν_2 are defined in (41). Simple computations reveal that $det(\boldsymbol{J}) = \frac{1}{\tau} \neq 0$.

The implicit function theorem guarantees that there exists a unique smooth function $x = x(q),\ y = y(q)$ defined on some interval $0 \leq q < q_0$ such that

$$\underline{\boldsymbol{Q}}(q, x(q), y(q)) = \boldsymbol{O} \tag{44}$$

with $x(0) = x^\star$ *and* $y(0) = y^\star$. *This means that the dynamical system (40) has a regular stationary point* $(x(q), y(q))$ *for* $0 < q < q_0$, *for which* $x(q) \to x^\star$, $y(q) \to y^\star$ *as* $q \to 0$.

Next, we investigate the existence of stationary points $(x(q), y(q))$ for the system (40) for small positive q, which converge (as $q \to 0$) to a singular stationary point (SSP) (x^*, y^*) in the sense of Definition 8. No SSP can belong to a transparent wall, while white walls can only contain unstable SSP. That is why we restrict ourselves to the case of SSP belonging to black walls. From Proposition 1 we know that the only possible black wall is L_i^1, where $x > \theta_e$ and $y = \theta_i$. Unlike Theorem 1, we now have not the exact value of the coordinate x^* of the SSP. The only a priori information we have is that $y^* = \theta_i$. This is, of course, an additional difficulty, which we overcome by replacing y with a new variable. This helps us to visualize the first coordinate of the SSP using the implicit function theorem. For convenience, we use below the following notation: $P_q = (x(q), y(q))$ $(q > 0)$, $P_0 = (x^*, y^*)$.

Theorem 2. *Assume that the system*

$$\mu_1 x + \omega_{ee} + \nu_1 \theta_i - \frac{\omega_{ei}}{\tau} Z_i = 0 \tag{45a}$$

$$\mu_2 x + \omega_{ie} + \nu_2 \theta_i - \frac{\omega_{ii}}{\tau} Z_i = 0 \tag{45b}$$

has a solution (x^*, Z_i^*) *satisfying the constraints* $x^* > \theta_e$, $0 < Z_i^* < 1$. *Then*

1. $\exists\ q_0 > 0$ *and* P_q *satisfying (44) for* $0 < q < q_0$.
2. $P_q \to P_0 \in L_i^1$ *as* $q \to 0$, *where*

$$P_0 = (x^*, \theta_i). \tag{46}$$

Proof. *As announced, we prove this theorem by using the implicit function theorem. But this theorem is not applicable for the equilibrium condition (44) due to the discontinuity of vector function* $\underline{\boldsymbol{Q}}$ *in the limit* $(q \to 0)$. *In order to overcome this problem, we express the equilibrium condition in terms of* x *and* Z_i *using the inverse Hill function*

$$y = H^{-1}(q, \theta_i, Z_i) = \theta_i \left(\frac{Z_i}{1 - Z_i} \right)^q. \tag{47}$$

The equilibrium condition (44) in the new variables x and Z_i is given by

$$\underline{\mathbf{f}}(q, x, Z_i) = \begin{bmatrix} f_e(q, x, Z_i) \\ f_i(q, x, Z_i) \end{bmatrix} = \begin{bmatrix} 0 \\ 0 \end{bmatrix}, \tag{48}$$

where

$$f_e(q, x, Z_i) = \mu_1 x + \nu_1 \theta_i \left(\frac{Z_i}{1 - Z_i} \right)^q + \omega_{ee} Z_e(x) - \frac{\omega_{ei}}{\tau} Z_i \tag{49a}$$

$$f_i(q, x, Z_i) = \mu_2 x + \nu_2 \theta_i \left(\frac{Z_i}{1 - Z_i} \right)^q + \omega_{ie} Z_e(x) - \frac{\omega_{ii}}{\tau} Z_i \tag{49b}$$

and $\left(\frac{Z_i}{1-Z_i}\right)^q \to 1$ $(0 < Z_i < 1)$, $Z_e(x) \to 1$ $(x > \theta_e)$ *as* $q \to 0$ *due to the properties of the Hill function. We then make the following observations*:

1. *The mapping* $\underline{\boldsymbol{f}} \colon [0, \infty) \times (\theta_e, \infty) \times (0, 1) \longrightarrow \mathbb{R} \times \mathbb{R}$ *is a smooth vector function.*

2. *By the assumption (45), there exists a point* $(0, x^*, Z_i^*) \in [0, \infty) \times (\theta_e, \infty) \times (0, 1)$ *such that* $\underline{\boldsymbol{f}}(0, x^*, Z_i^*) = \boldsymbol{O}$.

3. *The Jacobian* $\mathbf{J}_1$ *of the vector function* $\underline{\boldsymbol{f}}$ *evaluated at* $(0, x^*, Z_i^*)$ *is given as*

$$\mathbf{J}_1 = \begin{bmatrix} \frac{\partial f_1}{\partial x} & \frac{\partial f_1}{\partial Z_i} \\ \\ \frac{\partial f_2}{\partial x} & \frac{\partial f_2}{\partial Z_i} \end{bmatrix} (0, x^*, Z_i^*) = \begin{bmatrix} \mu_1 & \frac{-\omega_{ei}}{\tau} \\ \\ \mu_2 & \frac{-\omega_{ii}}{\tau} \end{bmatrix}. \tag{50}$$

Using (41) we easily obtain that

$$det(\boldsymbol{J}_1) = \frac{\omega_{ii}}{\tau}.$$

Since $\omega_{ii} > 0$ *by* (6), *the Jacobian* $\boldsymbol{J}_1$ *is therefore non-degenerate. Hence by the implicit function theorem there is a unique smooth solution* $Z_i = Z_i(q)$ *and* $x = x(q)$ *of* $\underline{\boldsymbol{f}}(q, x, Z_i) = \boldsymbol{O}$ *with* $Z_i(0) = Z_i^*$ *and* $x(0) = x^*$. *This solution corresponds to a point* P_q *with the coordinates* $(x_q,\ \theta_i(\frac{Z_i}{1-Z_i})^q)$ *approaching the point* P_0 *with the coordinates* (x^*, θ_i). *This point is a SSP.*

Remark 1. *The values x^* and Z_i^* in Theorem 2 can be calculated explicitly:*

$$x^* = \frac{\theta_i \omega_{ei} - d}{\omega_{ii}}, \qquad Z_i^* = \frac{\omega_{ie} + \theta_i}{\omega_{ii}}.$$

These formulae allow for a straightforward verification of the constraint assumptions put on the solution of the system (45).

6. Stability analysis of regular and singular stationary points

In this section we study asymptotic stability of regular (RSP) and singular (SSP) stationary points for the dynamical system (40). We first look at the stability of RSP and their perturbations.

Theorem 3. *Assume that the dynamical system (40) with $q = 0$ has a RSP $(x^\star, y^\star)$. Then it is asymptotically stable. Moreover, for small $q > 0$ the stationary points $(x(q), y(q))$ of the system (40) constructed in Theorem 1 are all asymptotically stable, too.*

Proof. *By Theorem 1 the stationary points $(x(q), y(q))$ exist for some q-interval about $q = 0$, where we also have continuous dependence on the parameter q. We now investigate the stability of the RSP by means of the invariants (trace and determinant) of the Jacobian $\boldsymbol{J}$ of (43), i.e.*

$$tr(\mathbf{J}) = T = -(1 + 1/\tau), \tag{51}$$

$$det(\mathbf{J}) = D = \mu_1\, \nu_2 - \mu_2\, \nu_1 = 1/\tau. \tag{52}$$

The stationary point is stable if $\boldsymbol{T} < 0$ and $\boldsymbol{D} > 0$ [8, 23]. *We always get $tr(\boldsymbol{J}) < 0$ and $det(\boldsymbol{J}) > 0$, because the time constant τ is strictly positive. We observe that the Jacobian $\boldsymbol{J}$ depends continuously on the steepness parameter q. Hence, there exists a small positive q_0 such that $tr(\boldsymbol{J}) < 0$ and $det(\boldsymbol{J}) > 0$ for $0 < q < q_0$, from which it follows that the stationary points $(x(q), y(q))$ are asymptotically stable for some q-interval about $q = 0$.*

Analysis of SSP again requires more technique than the above analysis of RSP. To this end, we need to determine the dynamics of the system (40) with $q = 0$ along the black walls, which we do by applying the singular perturbation analysis (SPA) [14, 23, 24]. The results of our investigations are summarized in the following theorem:

Theorem 4. *Under the assumptions of Theorem 2, the SSP $P_0 \in L_i^1$ given by (46) satisfies the following conditions:*

1. *P_0 is asymptotically stable.*
2. *The dynamics along the wall L_i^1 in a vicinity of P_0 are given as*

$$\frac{dx}{dt} = \mu_1\, x + \nu_1\, \theta_i + \omega_{ee} - \frac{\omega_{ei}}{\tau}\, \overline{Z}_i(x), \tag{53}$$

where

$$\overline{Z}_i(x) = \frac{\tau(\mu_2\, x\ + \nu_2\, \theta_i + \omega_{ie})}{\omega_{ii}}. \tag{54}$$

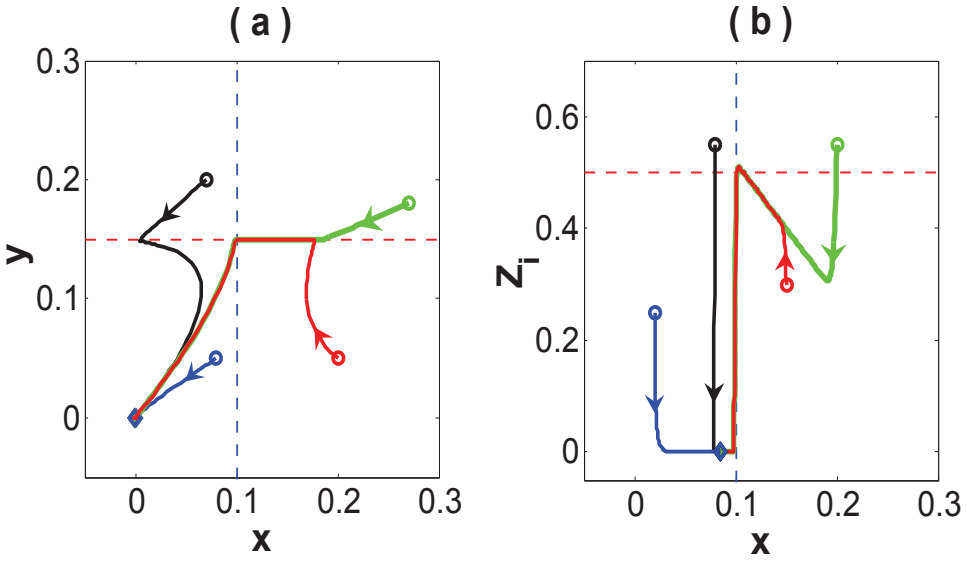

Figure 7: (a) Solutions of the system (40) with different initial conditions (circles) traced out with different color curves in the (x,y)-plane moving to the stationary point $(0, 0)$. (b) Solutions of the system (55) with different initial conditions (circles) traced out with different color curves in the (x, Z_i)-plane converging to the stationary point $(0.085, 0)$. The corresponding parameters are given by the parameter set D in Table 1. The standard MATLAB ODE solver (ode45) is used to demonstrate these results numerically for $q = 0.005$.

PROOF. *From Theorem 2 we know that SSP exists and belongs to the black (attracting) wall L_i^1. Therefore, it is natural to assume that the SSP will be asymptotically stable. However, a rigorous verification of this fact requires information about the dynamics along the wall, which cannot be calculated explicitly, as the right-hand side of the limit system (40) is discontinuous along the walls.*

Wishing to apply singular perturbation analysis, we transform the set of equations (40) to

$$x' = \mu_1\, x\ + \nu_1\, H^{-1}(q, Z_i, \theta_i) + \omega_{ee}\, Z_e(x) - \frac{1}{\tau}\, \omega_{ei}\, Z_i \tag{55a}$$

$$q\, Z_i' = \frac{Z_i(1-Z_i)}{H^{-1}(q, Z_i, \theta_i)}\{\mu_2\, x\ + \nu_2\, H^{-1}(q, Z_i, \theta_i) + \omega_{ie}\, Z_e(x) - \frac{1}{\tau}\, \omega_{ii}\, Z_i\} \tag{55b}$$

by means of the transformation

$$\begin{bmatrix} x \\ y \end{bmatrix} \longrightarrow \begin{bmatrix} x \\ Z_i \end{bmatrix}, \tag{56}$$

where Z_i and $H^{-1}(q, Z_i, \theta_i)$ are given by (7) and (47), respectively. The dynamical behavior of the solutions of the system (40)and (55) with different initial conditions are given in Fig. 7a and Fig. 7b, respectively. We introduce the stretching transformation

$$\zeta = \frac{t}{q} \tag{57}$$

and rewrite the system (55) *as*

$$\frac{dx}{d\zeta} = q\{\mu_1\, x\ + \nu_1\, H^{-1}(q, Z_i, \theta_i) + \omega_{ee}\, Z_e(x) - \frac{1}{\tau}\, \omega_{ei}\, Z_i\} \tag{58a}$$

$$\frac{dZ_i}{d\zeta} = \frac{Z_i(1-Z_i)}{H^{-1}(q, Z_i, \theta_i)}\{\mu_2 x + \nu_2\, H^{-1}(q, Z_i, \theta_i) + \omega_{ie} Z_e(x) - \frac{1}{\tau}\omega_{ii} Z_i\}. \tag{58b}$$

The system (58) is referred to as the boundary layer equation and the dynamical behavior of this system with different initial conditions is explained in Fig. 8a. The SPA now consists of letting $q \to 0$ and calculating the limit dynamics. In this limit, we obtain

$$\lim_{q\to 0} H^{-1}(q, Z_i, \theta_i) = \theta_i, \ \text{ and } \ , Z_e(x) \to 1 \tag{59}$$

if $0 < Z_i < 1$ *and* $x > \theta_e$. *Hence we get*

$$\frac{dx}{d\zeta} = 0 \tag{60a}$$

$$\frac{dZ_i}{d\zeta} = \frac{Z_i(1-Z_i)}{\theta_i}\{\mu_2 x + \nu_2\ \theta_i + \omega_{ie} - \frac{1}{\tau}\omega_{ii} Z_i\} \tag{60b}$$

to the leading order. The stationary points for the equation (58b) are given as

$$Z_i = 0, \quad Z_i = 1, \quad , Z_i = \overline{Z}_i = \frac{\tau(\mu_2\ x\ + \nu_2\ \theta_i + \omega_{ie})}{\omega_{ii}}. \tag{61}$$

Fig. 8b explains the dynamical behavior of the system (60) for different initial conditions with constant x. *Observe that* $\overline{Z}_i(x^*) = Z_i^* \in (0,1)$. *In a vicinity*

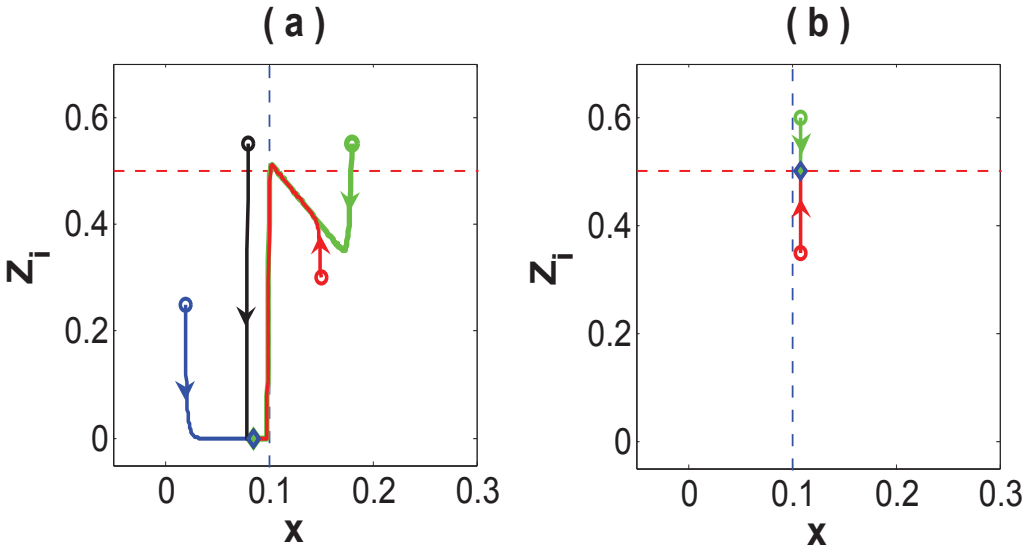

Figure 8: (a) Solutions of the system (58) with different initial conditions (circles) traced with different color curves in (x, Z_i)-plane for $q = 0.005$ converging to the stationary point $(0.085, 0)$(diamond). (b) Solutions of the system (60) with initial conditions $(0.11, 0.35)$ and $(0.11, 0.60)$ represented with red and green circles, respectively for $q \to 0$. The rest of the parameters are given by set D in the Table 1. The standard MATLAB ODE solver (ode45) is used to demonstrate these results numerically.

of x^*, we therefore have $\overline{Z}_i(x) \in (0,1)$. As $\omega_{ii} > 0$, the point $\overline{Z}_i$ is an isolated asymptotically stable stationary point for the equation (60b) with the attractor basin $(0,1)$. The equation (58a) in real time t *for $q \to 0$ gives therefore the following dynamics along the black wall L_i^1:*

$$\frac{dx}{dt} = \mu_1\, x + \nu_1\theta_i + \omega_{ee}\ - \frac{1}{\tau}\,\omega_{ei}\,\overline{Z}_i. \tag{62}$$

As $\overline{Z}_i(x^*) = Z_i^* \in (0,1)$, the point x^* becomes a (unique) stationary point for (60b). The coefficient of x can be calculated explicitly:

$$\mu_1 - \frac{\omega_{ei}}{\tau}\frac{\tau}{\omega_{ii}}\mu_2 = \frac{1}{\omega_{ii}}\,(\mu_1\omega_{ii} - \mu_2\omega_{ei}) = -1 < 0. \tag{63}$$

From (53), we then conclude that x^* is an asymptotically stable stationary solution of (60b), and P_0 is an asymptotically stable SSP for the system (40).

7. Conclusions and discussions

In the present work we have justified rigorously the approximation of the steep firing rate functions with a unit step function in a two-population neural firing rate model with steep firing rate functions. We have done this justification by exploiting the theory of switching dynamical systems. In this approach the phase space of the dynamical system should be divided into regular domains bounded by the singular (switching) domains. The examples of different types of singular domains for different choices of parameters involved in the model have been provided.

The explicit general conditions for attracting (black), repellent (white) and transparent walls have been derived (Proposition 1, Proposition 2 and Proposition 3). For each specific type of the singular domain, these propositions are conveniently expressed in terms of the parameters of the model: the connection strength ω_{mn} in the network and the threshold value θ_m for the firing action potentials.

On the basis of the results obtained in these propositions, some generic structure of the singular domains has been discovered. For instance, it has been found that only one of the four singular domains could be attracting, only two of the domains could be repelling and one domain would always be transparent. In addition, it has been shown that certain singular domains could

change their type for different values of the parameters of the system. In particular, the blackness condition requires that the excitatory-to-inhibitory connection strength must be greater than the inhibitory threshold, while the self inhibition connection plays the role of a control parameter. Hence, the connection strength in the network plays a decisive role for different types of the solution behavior close to the singular domains.

A special emphasis has been put on the problem of existence and asymptotic stability of the stationary regimes of the model. We have identified two different types of such regimes: regular (belonging to the continuity set of the simplified system where $q = 0$) and singular (belonging to the discontinuity set of the simplified system). We have offered explicit formulas for both types and demonstrated that in the generic situation the existence of the stationary regimes in the simplified model are preserved in the "real-world" model, at least for small $q > 0$. Finally, we have demonstrated, using the singular perturbation analysis technique, that the dynamics of the simplified model ($q = 0$) and the dynamics of the "real-world" model (for small $q > 0$) would always mimic each other. We have also explained how the simplified dynamics could be calculated explicitly.

Although the main results of the paper have been derived for the model with two populations of neurons, we stress that our analysis can be in a similar fashion performed for the N-population model as well. We also believe that our technique, combining with the general linear chain trick [8, 21], can be applied to the analysis of the dynamics of two or more population model for more complicated types of temporal kernels.

Finally, we would like to point out the possibility of applying the ideas in the present paper to networks with spatial structure. In a recent work by Oleynik et al [27] the justification of the unit step approximation of firing rate functions has been investigated by means of methods that are different from classic SPA (i.e. by nonlinear functional analysis and the degree theory). In a future investigation we intend to combine the methods of SPA with some ideas from Oleynik et al [27].

Acknowledgements

This work has been supported by The Research Council of Norway under the grant No. 178892: eNEURO-multilevel modeling and simulation of the nervous system (all authors), by Higher Education Commission of Pakistan (M. Yousaf) and by the research grants of the Norwegian University of Life Sciences (A. Ponosov, J. Wyller). The authors would also like to thank Dr. A. Machina and the PhD student V. Tafintseva for many fruitful and stimulating discussions during the preparation of this paper. The authors will also like to thank the reviewer for constructive remarks.

References

[1] P. Dayan and L.F Abbott, Theoretical Neuroscience, MIT press, Cambridge, MA 2001.

[2] H. R. Wilson, J. D. Cowan, A mathematical theory of the functional dynamics of cortical and thalamic nervous tissue, Kybernetik 13 (1973) 55-80.

[3] J. Wyller, P. Blomquist and G. T. Einevoll, On the origin and properties of two-population neural field models, a tutorial introduction, Biophysical reviews and letters 2 (2007) 79-98.

[4] E. M. Izhikevich, Dynamical Systems in Neuroscience: The Geometry of Excitability and Bursting, Th. MIT press, Cambridge, MA 2007.

[5] J. M. Bower and D. Beeman, The Book of Genesis: Exploring Realistic Neural Models with the General Neural Simulation System, 2nd edn. Springer, New York, NY, 1998.

[6] E. de Schutter, Computational Neuroscience-Realistic Modeling for Experimentalists, CRC Press, New York, NY, 2000.

[7] C. Koch and I. Segev, Methods in Neuronal Modeling, 2nd edn. MIT Press, Cambridge, MA, 1998.

[8] Ø. Nordbø, J. Wyller, G. T. Einevoll, Neural network firing rate models on integral form, Effect of temporal coupling kernel on equilibrium-state stability, Biol. Cybernetics 97 (2007) 195-209.

[9] G. B. Ermentrout, Neural networks as spatio-temporal pattern-forming systems, Rep. Prog. Phy. 61, (1998) 353-430.

[10] D. J. Pinto, A quantitative population model of whisker barrels: Re-examining the Wilson-Cowan equations, J. Comp. Neuroscience 3 (1996) 247-264.

[11] M. Tsodyks, W. Skaggs, T. Sejnowski and B. McNaughton, Paradoxical effects of external modulation of interneurons, J Neuro. 17 (1997) 4382-4388.

[12] T. Tateno, A. Harsch, H.P.C. Robinson,Threshold firing frequencycurrent relationships of neurons in rat somatosensory cortex: type 1 and type 2 dynamics, J. Neuro. 92 (2004) 2283-2294.

[13] I. Shlykova, A. Ponosov, Singular perturbation analysis and gene regulatory networks with delay, Nonlinear Analysis 72 (2010) 3786-3812.

[14] E. Plahte, S. Kjøglum, Analysis and generic properties of gene regulatory networks with graded response functions, Physica D: Nonlinear Phenomena 201 (2005) 150-176.

[15] H. D. Jong, J. L. Gouze, C. Hermandez, M. Page, T. Sari, J. Geiselmann, Qualitative simulation of genetic regulatory networks using piecewise linear models, Bull. Math. Bio. 66 (2004) 301-340.

[16] R. Thomas, Regulatory networks seen as synchronous automata: A logical description, J. Theor. Biol. 153 (1991) 1-23.

[17] A. Machina, A. Ponosov, Stability of stationary solutions of piecewise affine differential equations describing gene regulatory networks, J. Math. Anal. Appl. 380 (2011) 736-749.

[18] I. Shlykova, A. Ponosov, Y. Nepomnyashchikh, A. Shindiapin, General framework for stability analysis of gene regulatory networks with delay, Electronic J. of Diff. Equations 104 (2008) 1-36.

[19] L. Lu, R. Edwards, Structural principles for periodic orbits in glass networks, J. Math. Biology 60 (2010) 513 - 541.

[20] E. Plahte, T. Mestl, S. W. Omholt, A mathematical basis for description and analysis of systems with complex switch-like interactions, J. Math. Biology 36 (1998) 321-348.

[21] N. McDonald, Time lags in biological models: Lecture notes in Biomathematics, Springer Verlag, Berlin, Heidelberg, New York, 1978.

[22] J. M. Cushing, Integrodifferential Equations and Delay Models in Population Dynamics, Lecture Notes in Biomathematics, Springer, New York, NY, 1977.

[23] W. Wassov, Asymptotic expansions for ordinary differential equations, Dover publications New York (1965).

[24] A. B. Vasil'eva, V. F. Butuzov, L. V. Kalachev, The boundary function method for singular perturbation problems. SIAM Philadelphia, 1995.

[25] A. Ponosov, A. Shindiapin, Y. Nepomnyashchikh, Stability analysis of systems with switch-like interactions and distributed delays: A case study, Funct. Diff. Equations 13 (3-4) (2006) 539-570.

[26] E. Plahte, T. Mestl, S. W. Omholt, Global analysis of steady points for systems of differential equations with sigmoid interactions, Dyn. Stab. Syst. 9 (1994) 275-291.

[27] A. Oleynik, A. Ponosov and J. Wyller, On the properties of nonlinear nonlocal operators arising in neural field models, Submitted to Journal of Mathematical Analysis and Applications, 2012.